Flash melting of tantalum in a diamond cell to 85 GPa

Amol Karandikar and Reinhard Boehler

Phys. Rev. B **93**, 054107 — Published 9 February 2016

DOI: 10.1103/PhysRevB.93.054107

Flash-melting of tantalum in the diamond cell to 85 GPa.

Amol Karandikar,[1, 2, a)] and Reinhard Boehler[1]

[1] *Geophysical Laboratory, Carnegie Institution of Washington, 5251 Broad Branch Road NW, Washington D.C. 20015, U.S.A.*

[2] *Geowissenschaften, Goethe-Universität, Altenhöferallee 1, D-60438 Frankfurt a.M., Germany*

Abstract

We demonstrate a new level of precision in measuring melting temperatures at high pressure using laser flash-heating followed by Scanning Electron Microscopy and Focused Ion Beam Milling. The new measurements on tantalum put unprecedented constraints on its highly debated melting slope, calling for a reevaluation of theoretical, shock compression and diamond cell approaches to determine melting at high pressure. X-ray analysis of the recovered samples confirmed the absence of chemical reactions, which likely played a significant role in previous experiments.

Introduction

The unusually large discrepancies in the melting temperatures of tantalum (Ta) and some other transition metals at high pressures have challenged our understanding not only of the high temperature properties of metals relevant to bonding and structure, but also of our experimental

and theoretical approaches to determine melting temperatures at high pressure [1–17]. Particularly for Ta, the differences among static diamond cell results and shock experiments are too large to be explained by experimental errors, and a large spread in melting slopes from various theoretical results underlines the difficulties in predicting melting.

Most measurements on Ta melting in the laser-heated diamond cell (LHDAC) using optical and textural observations [1,18] and synchrotron X-ray diffraction (XRD) [19] have produced flat melting curves ($dT/dP \rightarrow 0$) with one exception [20]. Both shock data and theory have predicted steep but strongly varying melting slopes. Fig. 1 shows all results from static and shock experiments [21–23], and from theory [3,4,6,7,9,11,13,14,16,24].

There have been a number of suggestions to reinterpret the observation of low melting temperatures as being due to phase transitions from bcc to other energetically favorable but debated structures [10,15,16,25–29]. However, *in situ* XRD measurements in the DAC to 174 GPa at 300 K [31] and to 135 GPa, 5800 K [20] and calculations to 1 TPa at 0 K [30] have not reported any phase other than bcc.

The only methods for measuring melting at very high P-T conditions are shock measurements and the LHDAC technique. Problems associated with these techniques are the short time scale and chemical contamination of Ta, respectively. Previous LHDAC studies [1,18] that attributed melting to optical observations of textural changes on the sample surface lacked chemical analysis, and from our present observations, chemical contaminations of Ta during prolonged heating were highly likely in these studies. The *in-situ* XRD measurements in the LHDAC [20] that reported the only experimental steep melting curve relied on the appearance of a diffuse scattering ring and/or diffraction spots arising from fast recrystallization [20,32]. The main difficulty in such experiments is to confine and stabilize the melted portion of the sample

long enough to document melting. However, heating durations of even a few seconds near the melting temperature causes sample instabilities such as 'hole burning' and dispersion of melt into the surrounding pressure medium. These instabilities inevitably cause misalignment of the sample hotspot with the X-ray beam and the spectrometer to measure temperature, leading to large experiment uncertainties [20]. Moreover, the same XRD work reports chemical reactions to be unavoidable with the X-ray acquisitions lasting for a few tens of seconds during CW-heating.

Recent flash-heating technique in the LHDAC [33] circumvented these difficulties by reducing heating durations to milliseconds, yet measuring temperatures accurately. Sample recovery and subsequent analysis using Scanning Electron Microscopy (SEM) with Energy Dispersive X-ray Spectroscopy (EDX) unambiguously identified melting in the absence of chemical reactions and yielded accurate melting temperatures of rhenium and molybdenum at 1 atm and up to 50 GPa. In the present flash-heating work on Ta, we improved the measurement set up and extended the analysis using Focused Ion Beam Milling (FIBM) showing unambiguously the onset of melting and the extent of melt in depth. Here, we report precise melting measurements from 1 atm to 85 GPa without any sign of chemical alteration. Combining flash-heating with chemical, textural and depth-profile analysis of the recovered samples drastically reduced the experimental uncertainties compared to previous measurements.

Experimental

A Ta disc (diameter 25-45 μm, 5-8 μm thick), laser cut from a polished foil (Alfa Aesar 99.95% purity), resting on a plate of single crystal sapphire (3-5 μm thick, 40-60 μm wide) was placed on one of the diamond anvils. Re gaskets, pre-indented to 35 μm were used in a plate-DAC [34] with culet sizes 250-300 μm. The cells were loaded with 99.999 % purity argon as a pressure transmitting medium. Ruby grains (2-3 μm size) placed close to the sample served as pressure

markers. Above 35 GPa, the Raman signal of diamond was additionally used for pressure measurements [35]. Pressures measured before and after heating experiment did not differ by more than 2 GPa. We assume that the thermal pressure is low due to the small volume ratio of the heated sample portion to surrounding argon with low shear strength [36].

Fig. 2 schematically shows the optical set up for flash-heating in the diamond cell. An ytterbium fiber laser (λ=1070 nm, TEM_{00} mode, CW, IPG-Photonics), was triggered and modulated by a pulse generator (TENMA-TGP110) producing a rectangular pulse of 20 ms duration. The laser emission and the corresponding thermal response of the sample were measured by a photo diode (PD) and a photomultiplier tube (PMT), respectively (Fig. 2, iv). This heating duration is long enough to measure temperatures reliably and short enough to avoid chemical reactions or sample instability. The flash-heating and the temperature measurement were synchronized such that the thermal response of the sample during 20 ms is fully recorded by the spectrometer. The sample reached a constant temperature in less than 2 ms. The rise and fall times of the thermal response, monitored by a photomultiplier tube (PMT), contribute < 1% to the total spectral intensity. Further details of the optical set up and temperature measurement can be found elsewhere [33].

The procedure for the melting measurements was as follows: Microscope-images of the sample (Ta disc) were recorded before loading and after pressurizing to the desired pressure. For optical alignment, the laser power was adjusted to create a hotspot on the sample at temperatures below the ambient melting temperature of Ta to avoid any modification of the sample. Further, the laser-focus was adjusted (Fig. 2, i) to obtain a temperature gradient of < 10 K over the central area of the hot spot with 3 μm in diameter (Fig. 2, ii) from which the temperatures were measured with a calibrated CCD spectrometer. The sample was then heated with a higher laser

power in a single event of 20 ms (flash), while recording the temperature (Fig. 2, iii). Microscope-images of the sample were recorded after this event and after sample recovery. The recovered sample was then analyzed using SEM (JEOL-JSM-6500F and ZEISS-AURIGA-40) for surface texture and FIBM (ZEISS-AURIGA-40) for depth-profiling, measuring the extent of melt. Chemical analysis of Ta was done using EDX (JEOL-JSM-6500F) on the heated portions on the surface and in the interior exposed by FIB cuts. This procedure was repeated with new samples at a given pressure until, a temperature range was covered spanning about 400 K below and above a temperature at which a first smooth textured modification appeared in the heated area indicating melting (see discussion). Flash-heating runs were carried out at 20, 22, 32, 35, 50, 65 and 85 GPa (Fig. 8).

Results

To test the accuracy of the melting criterion and reproducibility of the results of the described heating procedure, we flash-heated a 30 μm thick polished Ta foil in an argon gas flow at 1 atmosphere below and above the known melting temperature of 3270 K [37,38] (Fig. 3). The argon environment prevented any detectable chemical reaction upon heating for all temperatures, as checked in the EDX, in stark contrast to experiments in air. The EDX instrument used can detect 0.1-0.2% of oxygen (O) and carbon (C) and at 25 keV the incident electron beam probes a depth of about 800 nm. In a separate comparative study using EDX conducted at 5, 15 and 25 keV, with the instrument calibrated using Ta standard specimen, the source of traces of O and C was found to be only from the surface and not in the bulk of the material.

At 3195 K, the first melt feature in the form of a crater is seen in the SEM image and at 3267 K, depth-profiling using FIBM showed restructuring of material several micrometers in

depth and diameter with a sharp boundary. We thus conclude that melting starts at 3195 K, but the amount of melt is too small to be visible in the depth profile compared to that for 3267 K. Given the age of the 1 atm literature melting temperatures, ranging from 3200-3300 K, we suggest a slight downward correction based on our more accurate calibration procedures [39].

As a melt-criterion at higher pressure, we thus use the first textural modification (onset of melting) as a lower bound of the melting temperature and the restructuring of the bulk material in depth as an upper bound. Typically, these bounds lie within 100 K for Ta.

Out of the total 71 runs carried out, we report 42 here. Discarded runs include test runs to optimize the laser power, laser defocusing and flash-heating duration, along with a few experimental runs with unsatisfactory Planck-fits, optical misalignment or suspected chemical impurity. To check the possible chemical contamination or structural modifications during sample preparation using laser-cutting, we carried out flash-heating test runs on samples prepared by FIBM and found no differences in the melting temperatures.

Fig. 4 shows microscope-pictures of Ta discs for two separate runs (A1→A4, B1→B4) before loading, before and after flash-heating at 35 GPa, and after recovery to ambient pressure. At 35 GPa and 3709 K there is no change after flash-heating, whereas at 3845 K, a shiny crater is formed. Samples recovered to ambient conditions from the same pressure but quenched from temperatures differing by ≅135 K show concave, rough features contrasting the convex, shiny smooth melt features. These samples were further analyzed using SEM, FIBM and EDX probes (Fig. 5). In contrast to the unchanged textural appearance to several micrometers in depth at 3709 K, the FIB cross-section at 3845 K shows a clear boundary separating the unmolten and the restructured quenched molten portion. EDX at 25 keV on these samples revealed no chemical reaction upon flash-heating.

As another example of flash-heating, Fig. 6 shows two separate runs (2 vertical panels) on two different samples loaded in the DAC at 50 GPa. The microphotographs of Ta discs before (A, B) and after flash-heating (A', B') show that at 3906 K there is no change after flash-heating, whereas at 3975 K, a shiny crater is formed. Likewise the 35 GPa run, the convex, shiny smooth melt features contrasting the concave, rough, 'solid' features are retained upon recovery to ambient conditions. The further analysis using the SEM and FIBM reveals that in contrast to the cross-section at 3906 K (a'), the one at 3975 K (b') shows a clear boundary between the unmolten and the restructured quenched molten portion. EDX on these samples confirmed an absence of chemical reactions. The described FIB-profiles at 35 and 50 GPa, shown in Fig. 7 for clarity, reveal the extent of melt to several micrometers in depth.

SEM and EDX were performed for all 42 runs and FIBM was done whenever depth profiling was required. In Fig. 8, the P-T conditions leading to no textural modifications are assigned as 'solid', those showing melt features to several micrometers in depth are 'molten', and those with textural modification on the surface are 'onset' representing the lower bound of the melting curve as discussed above. We report the melting temperature in fig. 1 corresponding to the 'onset' with an uncertainty equal to the difference between the highest 'solid' temperature and the lowest 'molten' temperature. The data at 85 GPa show melt features only at 4318 K (Fig 9, b) due to insufficient number of runs, and from the uncertainties in the lower pressure runs, we conclude that the melting curve must lie within ±100 K of this temperature.

Discussion

The differences between the present and previous LHDAC results may be explained as follows: The previously used laser speckle method [1] attributes the onset of melting to laser-speckle

motion due to textural changes of the sample surface during melting. It has been reliably used for many materials from different classes. Yet, for Ta, it underestimated the melting temperature e.g. by 500 K at 85 GPa (Fig. 1). Such a large discrepancy cannot be explained by experimental uncertainties and must therefore be due to chemical contamination caused by long heating durations [20]. The same applies for the earlier XRD measurements [19].

With regards to the large uncertainties in melting temperatures reported from the recent LHDAC-XRD experiments [20] we conclude that these must have been due to a combination of misalignment due to sample instabilities while measuring temperatures as discussed earlier, and chemical reactions of the sample reported in that study itself. In the absence of sample instabilities and contaminations, the XRD measurements on their 5 μm thick samples using double-sided heating should have been able to detect the substantial melt portion as evident from our figure 7.

Conclusion

In contrast to the recent melting measurements on tantalum, which showed large uncertainties, the present melting curve cannot be reconciled with shock measurements and theoretical predictions. Flash-heating combined with SEM, FIBM and EDX analysis on the recovered samples produced significantly more accurate data to 85 GPa than previous melting experiments with melting temperatures bracketed within ±100 K. The textural modifications are very reproducible and unambiguous, and chemical contaminations are carefully monitored for the first time to ensure sample purity. The present work solves the two major problems in melting experiments: detection of the onset of melting and chemical contamination.

Acknowledgments

This work was supported as part of Energy Frontier Research in Extreme Environments Center (EFree), an Energy Frontier Research Center funded by the U.S. Department of Energy, Office of Science under Award Number DE-SC0001057. Carnegie-DOE Alliance Center, Grant DE-NA0002006 funded in part. We thank Y. Meng, R. Hrubiak, T. Strobel, M. Guthrie, B. Haberl for XRD measurements and C. Crispin and J. Armstrong for their help in FIBM and SEM.

References

[a] author for correspondence : akaran@carnegiescience.edu

[1] D. Errandonea, B. Schwager, R. Ditz, C. Gessmann, R. Boehler, and M. Ross, Phys. Rev. B **63**, 132104 (2001).

[2] J. Moriarty, Phys. Rev. B **49**, 12431 (1994).

[3] Y. Wang, R. Ahuja, and B. Johansson, Phys. Rev. B **65**, 014104 (2001).

[4] J. Moriarty, J. Belak, R. Rudd, P. Söderlind, F. Streitz, and L. H. Yang, J. Phys. Condens. Matter **14**, 2825 (2002).

[5] A. Belonoshko, S. Simak, A. Kochetov, B. Johansson, L. Burakovsky, and D. Preston, Phys. Rev. Lett. **92**, 195701 (2004).

[6] A. Strachan, T. Ça□in, O. Gülseren, S. Mukherjee, R. Cohen, and W. Goddard III, Model. Simul. Mater. Sci. Eng. **12**, S445 (2004).

[7] A. K. Verma, R. S. Rao, and B. K. Godwal, J. Phys. Condens. Matter **16**, 4799 (2004).

[8] C. Cazorla, M. J. Gillan, S. Taioli, and D. Alfè, J. Chem. Phys. **126**, 1 (2007).

[9] M. Foata-Prestavoine, G. Robert, M. Nadal, and S. Bernard, Phys. Rev. B **76**, 104104 (2007).

[10] M. Ross, D. Errandonea, and R. Boehler, Phys. Rev. B **76**, 184118 (2007).

[11] S. Taioli, C. Cazorla, M. Gillan, and D. Alfè, Phys. Rev. B **75**, 214103 (2007).

[12] A. Belonoshko, L. Burakovsky, S. Chen, B. Johansson, A. Mikhaylushkin, D. Preston, S. Simak, and D. Swift, Phys. Rev. Lett. **100**, 135701 (2008).

[13] Z. Liu, L. Cai, X. Chen, and F. Jing, Phys. Rev. B **77**, 024103 (2008).

[14] F. Xi and L. Cai, Phys. B **403**, 2065 (2008).

[15] C. Wu, P. Söderlind, J. Glosli, and J. Klepeis, Nat. Mater. **8**, 223 (2009).

[16] L. Burakovsky, S. Chen, D. Preston, A. Belonoshko, A. Rosengren, A. Mikhaylushkin, S. Simak, and J. Moriarty, Phys. Rev. Lett. **104**, 255702 (2010).

[17] Z. Zeng, C. Hu, X. Liu, L. Cai, and F. Jing, Appl. Phys. Lett. **99**, 191906 (2011).

[18] J. Ruiz-Fuertes, A. Karandikar, R. Boehler, and D. Errandonea, Phys. Earth Planet. Inter. **181**, 69 (2010).

[19] D. Errandonea, M. Somayazulu, D. Häusermann, and H. Mao, J. Phys. Condens. Matter **15**, 7635 (2003).

[20] A. Dewaele, M. Mezouar, N. Guignot, and P. Loubeyre, Phys. Rev. Lett. **104**, 255701 (2010).

[21] J. M. Brown and J. W. Shaner, in *Shock Waves Condens. Matter - 1983*, edited by J. R. Asay, R. A. Graham, and G. K. Straub (Elsevier Science Publishers B. V., 1984), pp. 91–94.

[22] C. Dai, J. Hu, and H. Tan, J. Appl. Phys. **106**, 043519 (2009).

[23] J. Li, X. Zhou, J. Li, Q. Wu, L. Cai, and C. Dai, Rev. Sci. Instrum. **83**, 053902 (2012).

[24] J. Haskins, J. Moriarty, and R. Hood, Phys. Rev. B **86**, 224104 (2012).

[25] L. Hsiung and D. Lassila, Scr. Mater. **39**, 603 (1998).

[26] Y. Yao and D. Klug, Phys. Rev. B **88**, 054102 (2013).

[27] Z. Liu, L. Cai, X. Zhang, and F. Xi, J. Appl. Phys. **114**, 73520 (2013).

[28] J. Hu, C. Dai, Y. Yu, Z. Liu, Y. Tan, X. Zhou, H. Tan, L. Cai, and Q. Wu, J. Appl. Phys. **111**, 033511 (2012).

[29] P. Rigg, R. Scharff, and R. Hixson, J. Phys. Conf. Ser. **500**, 032018 (2014).

[30] P. Söderlind and J. Moriarty, Phys. Rev. B **57**, 10340 (1998).

[31] H. Cynn and C. Yoo, Phys. Rev. B **59**, 8526 (1999).

[32] A. Dewaele, M. Mezouar, N. Guignot, and P. Loubeyre, Phys. Rev. B **76**, 144106 (2007).

[33] L. Yang, A. Karandikar, and R. Boehler, Rev. Sci. Instrum. **83**, 063905 (2012).

[34] R. Boehler, Rev. Sci. Instrum. **77**, 115103 (2006).

[35] Y. Akahama and H. Kawamura, J. Appl. Phys. **96**, 3748 (2004).

[36] R. Boehler, M. Ross, P. Söderlind, and D. B. Boercker, Phys. Rev. Lett. **86**, 5731 (2001).

[37] L. Malter and D. Langmuir, Phys. Rev. **55**, 743 (1939).

[38] J. Shaner, G. R. Gathers, and C. Minichino, High Temp. Press. **9**, 331 (1977).

[39] R. Boehler, Hyperfine Interact. **128**, 307 (2000).

[40] N. S. Fateeva and L. F. Vereshchagin, Sov. Phys. DOCKLADY **16**, 322 (1971).

[41] R. Boehler, H. Musshoff, R. Ditz, G. Aquilanti, and A. Trapananti, Rev. Sci. Instrum. **80**, 045103 (2009).

Figure captions:

Fig. 1: (color online) **Ta melting from theory, static and shock data to date.**

Theory: Generalized Lindemann: — [3], Dislocation mediated: --▼-- [7]; □ [14], Vacancy formation enthalpy: —*— [6], Quantum atomistic: ▪▪▪ [4], First principles DFT-GGA/PAW: --×-- [11], Co-existence phase MD : —●— EFS; —○— FM; ○ LREP [13], Ab-initio MD: bcc ◑; hex-ω ◐ [16], , DFT MGPT MD: ▲ [24]. STATIC data: 1 atm ◆ [37,38], Drickamer piston cylinder ✳ [40], Speckle method ▲ [1], bead formation: ● [1]; ● [18], XRD: ■ [19]; ■ [20], Laser power anomaly: ▼ [9]. SHOCK data: T calculated with heat capacity models: ☆ [21], T pyrometric: ☆ [22], Simultaneous Hugoniot-T measurement: ☆ [23]. Vertical dashed lines indicate predicted phase transition pressures for Hex-Ω [16], P_{nma} [26, 27] and an unidentified speculated phase [10]. Phase boundary between bcc and shear induced plastic flow: + [15]. ●: The flash-melting data measured in this work. The symbol size is larger than the individual uncertainty. Black dotted line is a guide to an eye.

Fig. 2: (color online) **Schematics of the experimental set up for single-flash heating in the LHDAC.**

A Graphic User Interface [GUI] command opens the shutter of the spectrometer to measure temperature and simultaneously triggers a pulse generator [PG] that controls the heating laser to produce a 20 ms rectangular pulse. A pair of achromats (ac) collects the thermal radiation from the central area (dia ≅3 μm) of the hot spot (inset i), which is aligned to the pinhole at the spectrometer entrance. Temperature profiles measured across the hot spot (inset ii) shows

gradients of < 10K over the central area. An infrared filter (IRf) and neutral density filters (ndf) filter out laser radiation and avoid oversaturation of the spectrometer, respectively. An iris minimizes chromatic aberration [41], allowing accurate temperature measurement in the wavelength range 450-900 nm (inset iii) using a CCD. A photo diode (PD) and a photomultiplier tube (PMT) (inset iv) record the 20 ms laser pulse and corresponding thermal response from the sample, respectively

Fig. 3: **Ta foil, flash-heated in argon flow at 1 atm, probed by SEM, FIBM and EDX.**

Row 1: SEM images of different flash-heated areas at increasing temperatures. Scale shown is for the entire row. At 3195 K the first textural modification is observed. Row 2: Respective FIB cross-sections cut across the features shown in row 1. For simplicity, only halve the cross-sections are shown. The modification at 3195 K is too small to identify any features in depth. At 3267 K, close to the known melting point of Ta (3270 K), a crater formed showed substantial restructuring of material with about 3 μm deep sharp boundary between unmolten solid and quenched liquid. Spots heated below 3195 K showed no textural change in their FIB profiles, whereas those above 3267 K show restructuring of the sample with a sharp boundary growing both laterally and in depth, with increasing temperature. Row 3: EDX spectra from unheated and heated portions indicating absence of any chemical reaction at and above melting.

Fig, 4: (color online) **Microphotographs of Ta discs at different stages of two separate flash-heating runs at 35 GPa.**

a1, b1: Ta discs placed on thin sapphire plates at 1 atm. a2, b2: Same discs loaded to 35 GPa in the DAC before heating. a3, b3: discs after flash-heating to 3709 K, 3845 K, respectively. In b3,

formation of a shiny, smooth circular crater was observed, in contrast to a3. a4, b4: Features retained on the discs recovered from the respective high P-T conditions. Scale bars shown are for the respective rows.

Fig. 5: **Ta discs, recovered from two separate flash-heating runs at 35 GPa, as probed by SEM, FIBM and EDX.**

a, b: SEM images of discs heated to 3709 K and 3845 K, respectively. The difference between the surface textures for these temperatures is significant and the melt features are similar to the one atmosphere test. Respective FIB cross sections a', b' are cut through the hot spot areas. No change in textural appearance in the depth in (a') contrasts a sharp boundary in (b'), extending a few micrometers in depth, separating quenched liquid and the unmolten solid. Respective EDX spectra a", b" indicate no chemical alteration upon melting. Scale bars shown are for the respective vertical panels.

Fig. 6: (color online) **Optical, SEM, FIBM and EDX analysis of Ta discs in two separate flash-heating runs at 50 GPa.**

The two vertical panels pertain to two separate runs. Row 1: Microphotographs of Ta discs placed on thin sapphire plates loaded to 50 GPa in argon in the DAC before heating (A, B) and after flash-heating to 3906 K, 3975 K (A', B'), respectively. In B', formation of a shiny, smooth circular crater was observed, in contrast to A'. a, b: SEM images of the recovered discs. The difference between the surface textures is significant and the melt features are similar to the 1 atm test (Fig. 2). a', b' : SEM images of the respective FIB cross-sections cut through the hot spot areas. Unaltered textural appearance in depth in a' contrasts a sharp boundary in b',

extending a few micrometers in the depth, separating the quenched liquid and the unmolten solid. A", b": Respective EDX spectra indicate no chemical alteration upon melting.

Fig. 7: **FIB cross sections of Ta discs recovered from (a) 35 GPa, 3845 K and (b) 50 GPa, 3975 K showing the extent of the molten portions.**

Fig. 8: (color online) **Flash-heating data on Ta in the LHDAC.**

Each data point is the result of a single flash-heating event on a new Ta disc. ◇ : 'solid'– no textural modifications observed on the surface and in depth of material. △ : 'onset' - the first melt features appeared. ● : 'molten'- restructuring of material observed with quenched liquid-solid boundary extending to several micrometers deep. At 85 GPa, only the 'onset' and 'solid' data were measured. The 'solid' data point lies on the previous flat melting data [1,19]. The dashed line is a guide to an eye.

Fig. 9: (color online) **Microphotographs of Ta at 85 GPa in the LHDAC.**

At 85 GPa, a Ta disc resting on a sapphire plate in argon in the DAC is shown before heating (a) and after flash-heating to 4317 K (b). The smooth crater in b clearly indicates melting.

Fig. 1

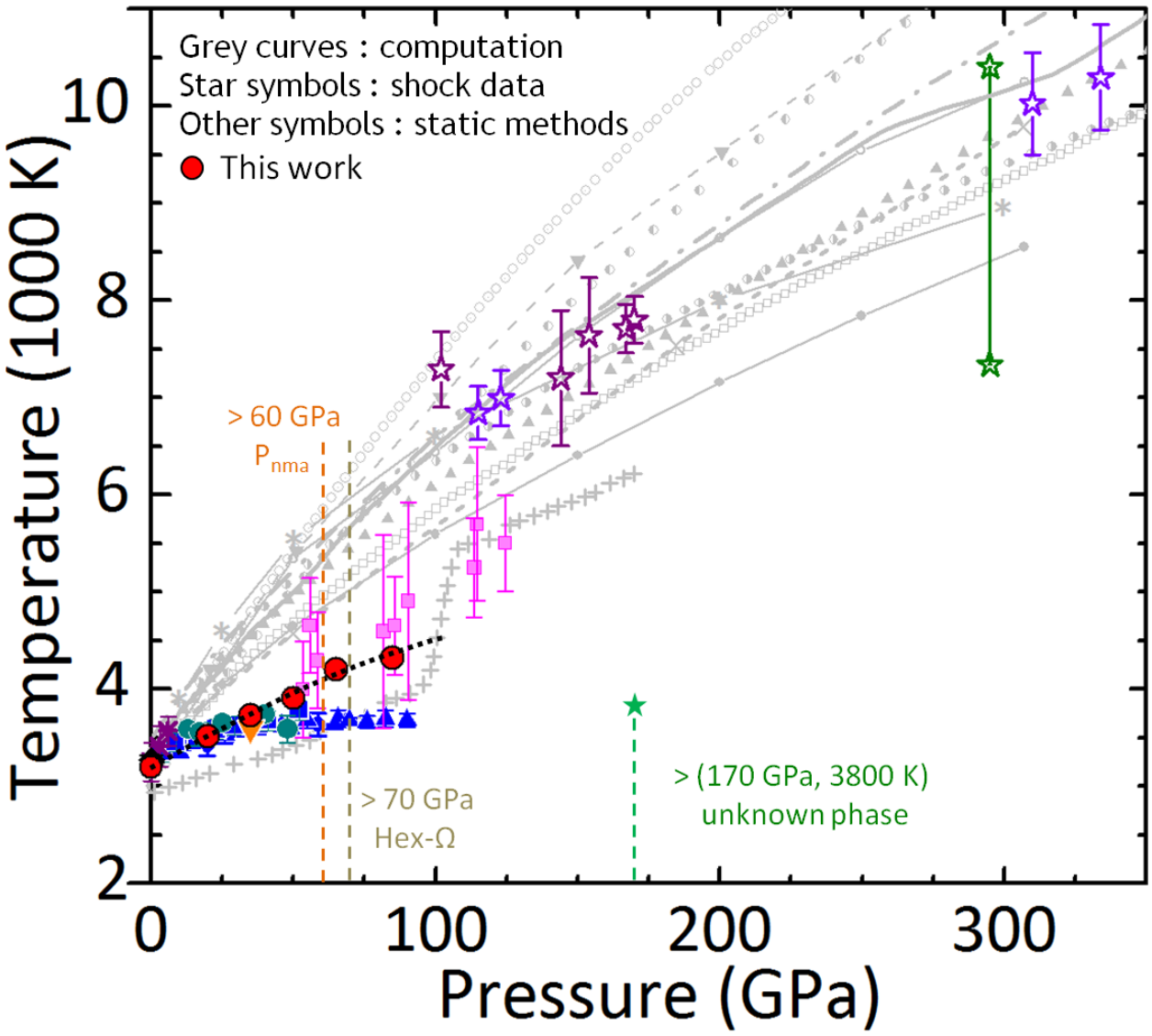
Grey curves : computation
Star symbols : shock data
Other symbols : static methods
This work
> 60 GPa
P nma
> 70 GPa
Hex-Ω
> (170 GPa, 3800 K)
unknown phase
Temperature (1000 K)
Pressure (GPa)
2
4
6
8
10
0
100
200
300

Fig. 2

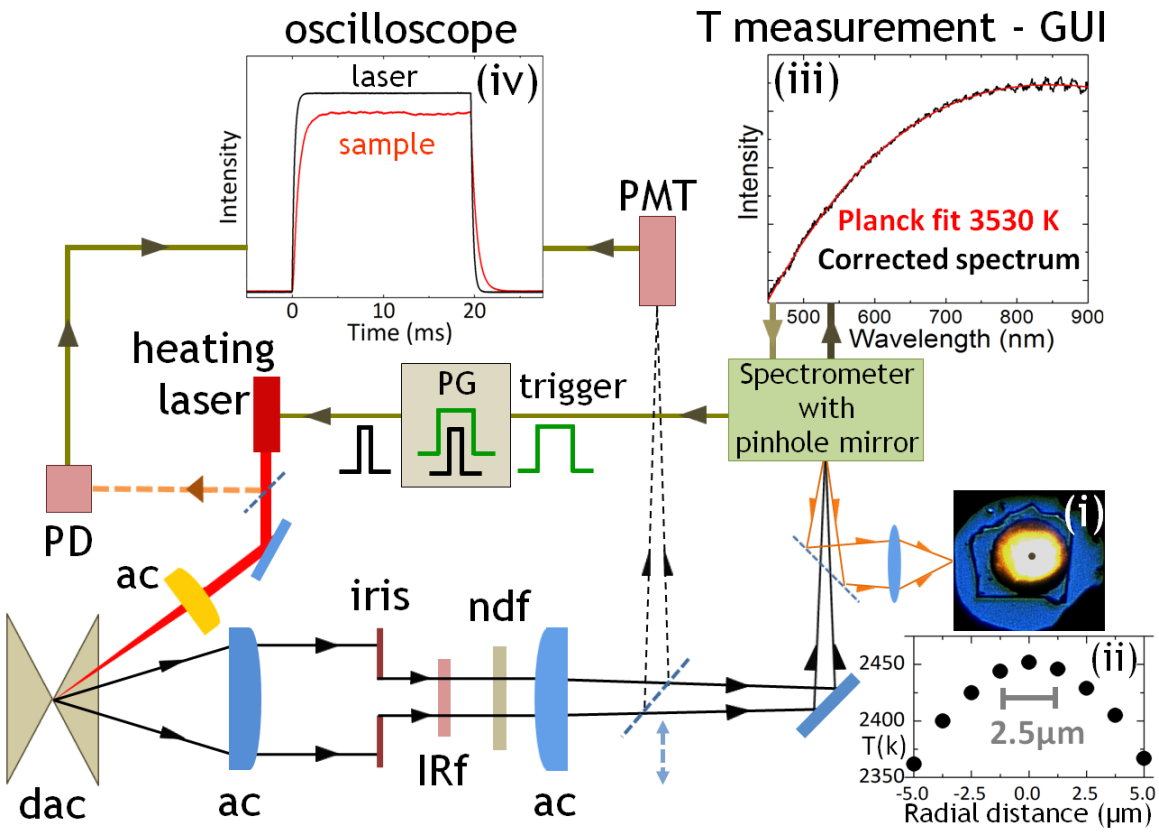
oscilloscope
T measurement - GUI
laser
sample
(iv)
Intensity
0
10
20
Time (ms)
PMT
(iii)
Intensity
Planck fit 3530 K
Corrected spectrum
500
600
700
800
900
Wavelength (nm)
heating
laser
PG
trigger
Spectrometer
with
pinhole mirror
PD
ac
iris
ndf
(i)
(ii)
2450
2400
T(k)
2350
2.5µm
-5.0
-2.5
0.0
2.5
5.0
Radial distance (µm)
dac
ac
IRf
ac

Fig. 3

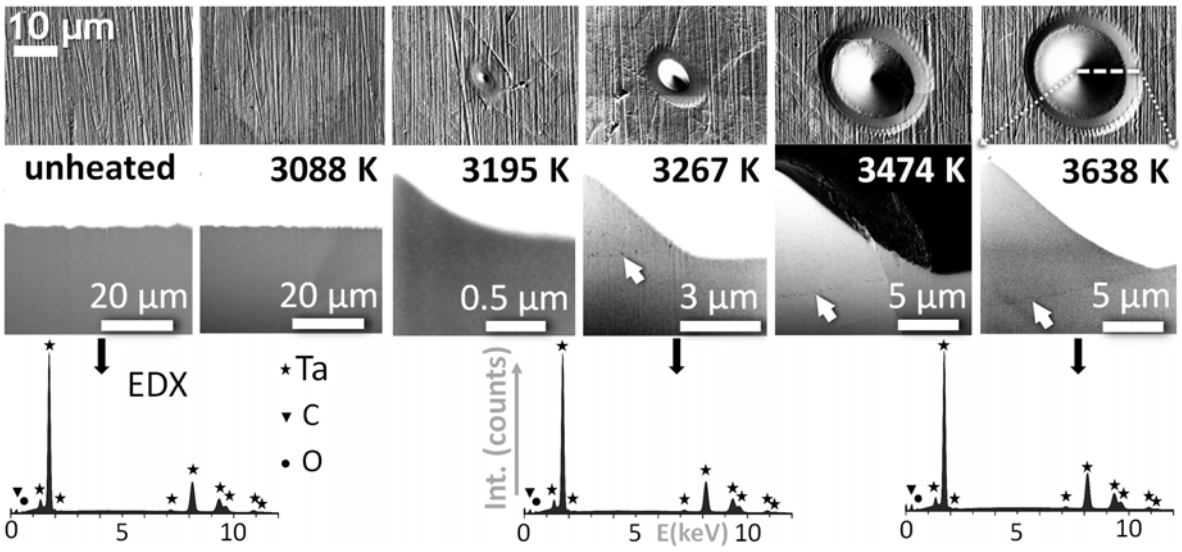
10 µm
unheated
3088 K
3195 K
3267 K
3474 K
3638 K
20 µm
20 µm
0.5 µm
3 µm
5 µm
5 µm
EDX
Ta
C
O
Int. (counts)
0
5
10
E(keV)

Fig. 4

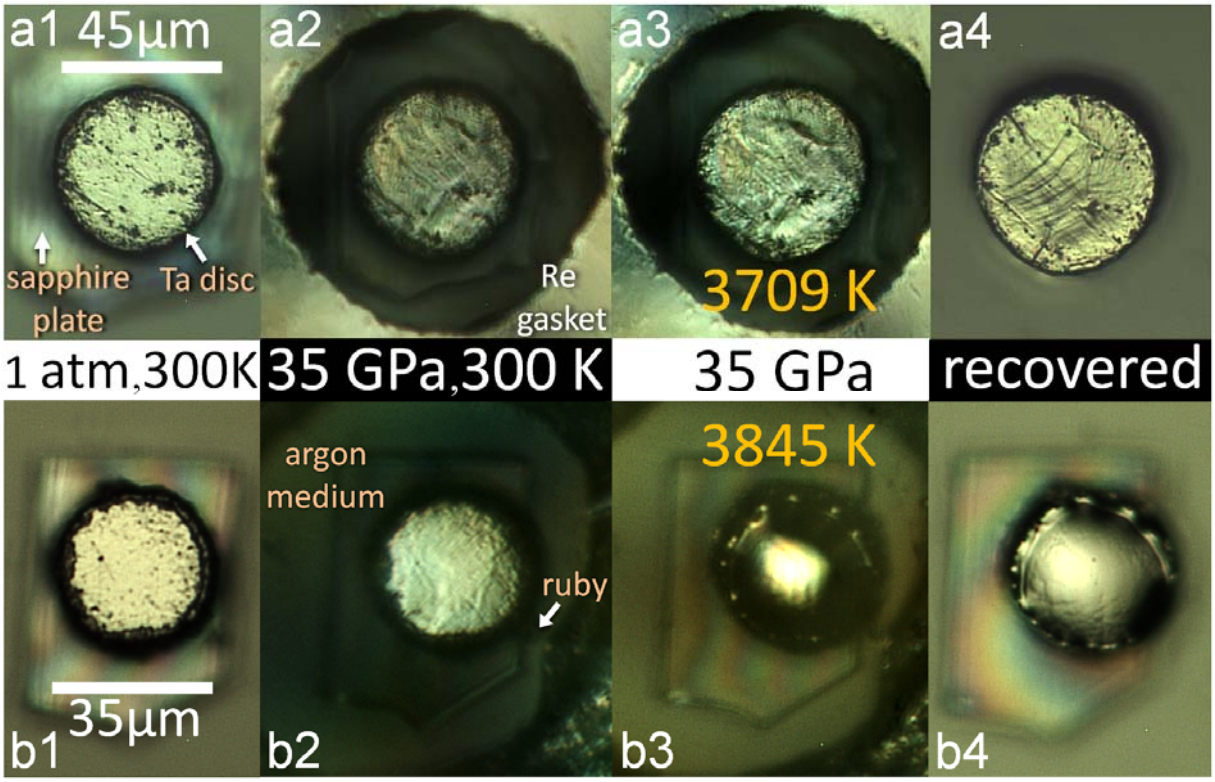
a1 45μm
sapphire plate
Ta disc
a2
Re gasket
a3
3709 K
a4
1 atm,300K
35 GPa,300 K
35 GPa
recovered
argon medium
ruby
3845 K
35μm
b1
b2
b3
b4

Fig. 5

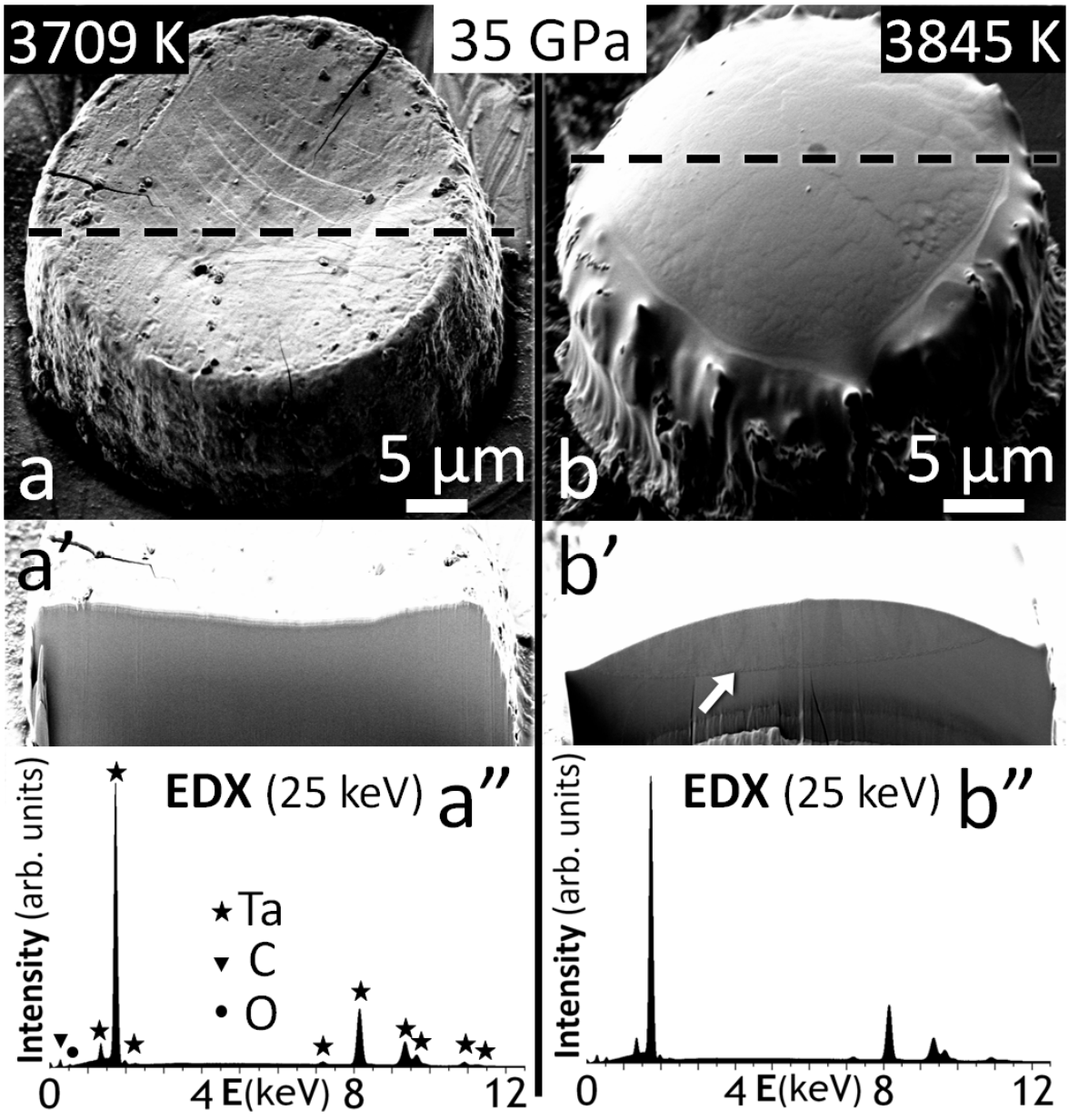
3709 K
35 GPa
3845 K
a
5 μm
b
5 μm
a'
b'
EDX (25 keV) a"
Ta
C
O
Intensity (arb. units)
0
4 E(keV) 8
12
EDX (25 keV) b"
Intensity (arb. units)
0
4 E(keV) 8
12

Fig. 6

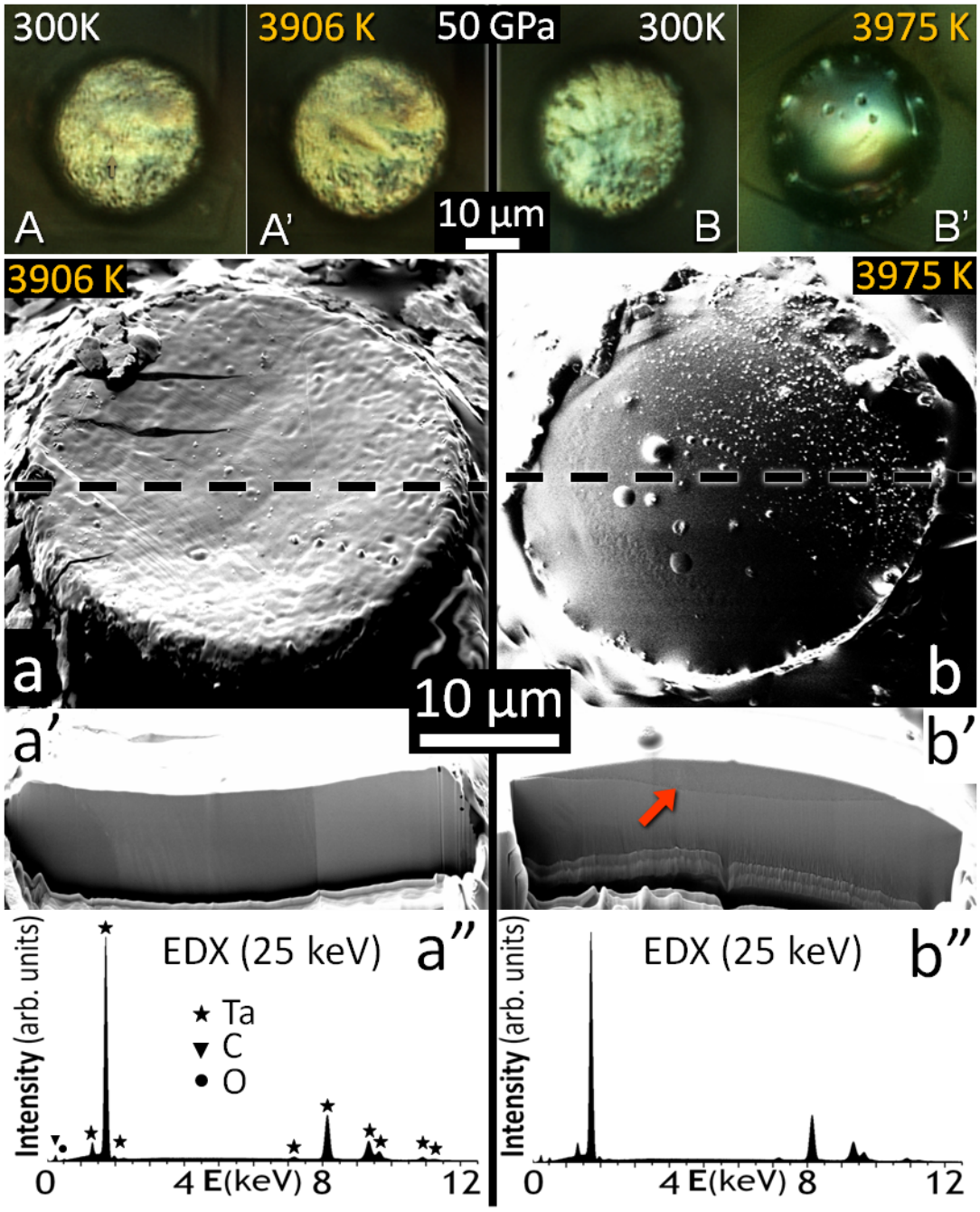
300K
3906 K
50 GPa
300K
3975 K
A
A'
10 µm
B
B'
3906 K
3975 K
a
b
10 µm
a'
b'
EDX (25 keV)
a"
Ta
C
O
Intensity (arb. units)
0
4 E(keV) 8
12
EDX (25 keV)
b"
Intensity (arb. units)
0
4 E(keV) 8
12

Fig. 7

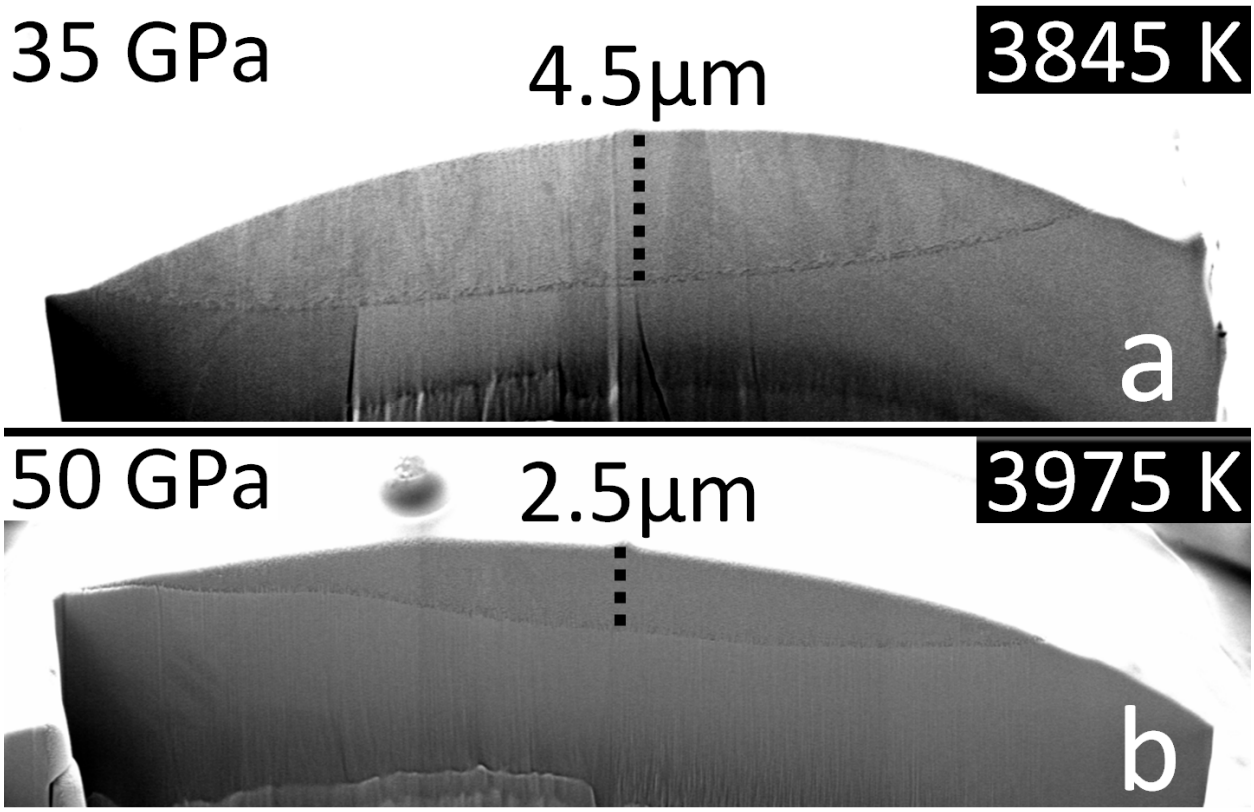

Fig. 8

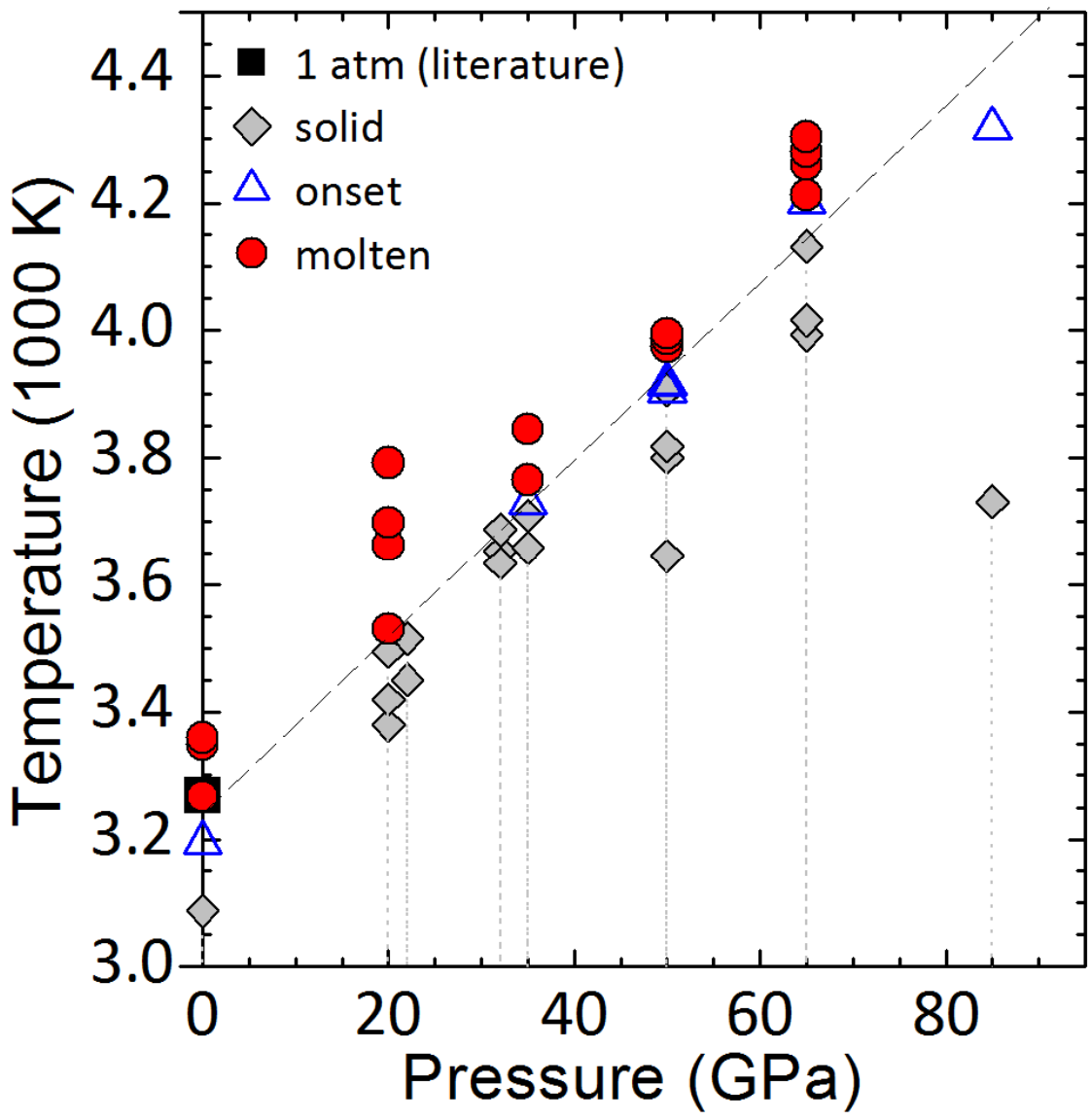
1 atm (literature)
solid
onset
molten
Temperature (1000 K)
Pressure (GPa)
4.4
4.2
4.0
3.8
3.6
3.4
3.2
3.0
0
20
40
60
80

Fig. 9